Pressure dependence of vibrational, thermal, and elastic properties of ZnSe: An *ab initio* study

I. Hamdi and M. Aouissi
Département de physique, Faculté des Sciences de Tunis, Campus Universitaire, 2092 Tunis, Tunisia

A. Qteish
Department of Physics, Yarmouk University, 21163 Irbid, Jordan

N. Meskini
Département de physique, Faculté des Sciences de Tunis, Campus Universitaire, 2092 Tunis, Tunisia
(Received 19 August 2005; revised manuscript received 6 March 2006; published 19 May 2006)

The density functional perturbation theory is employed to study the vibrational, thermal (within the quasiharmonic approximation) and elastic properties of ZnSe, and their pressure dependence up to transition pressure. The calculations are performed using a pseudopotential plane wave method and local density approximation for the exchange-correlation (XC) potential. The semicore Zn 3*d* electrons are treated as valence states. For comparison, nonlinear XC core corrections calculations are also performed, at zero pressure. Our results for the above properties are generally speaking in good agreement with experiment and with similar theoretical calculations, performed mostly at zero pressure. The linear thermal expansion is predicted to have strong pressure dependence, and the temperature range in which it has negative values increases with pressure. The heat capacity at constant pressure is predicted to have weak pressure dependence.

DOI: 10.1103/PhysRevB.73.174114 PACS number(s): 65.40.De, 62.20.Dc, 63.20.−e

I. INTRODUCTION

Since the demonstration of blue-green lasers fabricated from ZnSe and its alloys,[1] wide-band-gap semiconductors have received and still receiving considerable attention. In these important applications, epitaxially grown thin films of these materials are usually used. In this work we will focus mainly on the vibrational and thermal properties of ZnSe under normal and high pressures (P). The thermal properties are one of the most basic properties of any material. Thermal expansion is connected not only with thermal properties (thermal conductivity, specific heat, etc.) but also it influences many other properties, such as the temperature (T) variation of the energy band gap. Moreover, the knowledge of the thermal expansion coefficient is especially important for epitaxial growth.

Experimentally, the phonon spectra of ZnSe (at zero P) have been determined using inelastic neutron scattering (INS) by Hennion *et al.*[2] Employing Raman spectroscopy, Lin *et al.*[3] have measured the frequency of the optical phonon modes at the Γ point, as well as the P variation of the frequency and Grüneisen parameter of these modes. Using ^{67}Zn Mössbauer spectroscopy, Karzel *et al.*[4] have measured the P dependence of the Lamb-Mössbauer factor (LMF) of ZnSe. The observed decrease in LMF of ZnSe above 6.1 GPa has been attributed to a softening of phonon modes well below the transition pressure (P_t=13.5 GPa). The thermal properties of ZnSe have only been investigated by two quite old experiments.[5,6] Moreover, there is a significant discrepancy between their results for the linear thermal expansion at low T, below 60 K.

Several calculations have been performed to study the dynamical properties of ZnSe, at zero and high pressures. The thermal properties of ZnSe (at zero P) are investigated in a few of them. These calculations can be classified into three categories: (i) Model calculations, using the rigid-ion (RIM11)[7] and the adiabatic bond charge (ABCM) models.[8] The RIM11 model is used to calculate the phonon spectra (at zero and 13.7 GPa pressures), Grüneisen parameter and linear thermal expansion coefficient by Talwar *et al.*[7] In these calculations no softening of phonon modes has been obtained. The ABCM model is utilized[8] to calculate the phonon spectra and specific heat of ZnSe at zero P. (ii) *Ab initio* frozen-phonon calculations of the frequency of the phonon modes at the Γ and X points, using full-potential linear muffin-tin orbital (LMTO),[9] linear-augmented plane-wave (LAPW),[10] and SIESTA (pseudopotential localized orbitals)[10] methods. (iii) Density functional perturbation theory (DFPT) calculations.[11–20] This approach is used to study the phonon spectra,[21] Grüneisen parameter and linear thermal expansion coefficient[22] of ZnSe at zero P. However, in these calculations the semicore Zn 3*d* electrons are treated as part of the frozen core, and nonlinear exchange-correlation core corrections[23] (NLCCs) are included (hereafter these calculations will be referred to simply as NLCC).

The main aim of work is to provide a thorough DFPT investigation of the vibrational, thermal, and elastic properties of ZnSe, at zero and high pressures. The calculations are performed by using a pseudopotential plane-wave approach (PPPW) and the local density approximation (LDA) for the exchange-correlation potential. The semicore Zn 3*d* electrons are treated as valence states (hereafter these calculations will be referred to as 3*d*). For a better comparison with previous theoretical results, some NLCC calculations are also performed for ZnSe at zero pressure. The thermal properties are obtained within the quasiharmonic approximation. Moreover, the Born effective charge and the high-frequency static dielectric constant are also calculated as functions of P.

This paper is organized as follows. In Sec. II, a short outline of the used theoretical approach and computational details are given. In Sec. III, our results are presented and

discussed in comparison with the available experimental data and other theoretical results. Finally, the main results and conclusions are summarized in Sec. IV.

II. THEORY

A. Lattice dynamics: Interatomic force constants approach

The interatomic force constants (IFC's) describing the atomic interactions in a crystalline solid are defined in real space as[19]

$$C_{\kappa\alpha,\kappa'\beta}(a,b) = \frac{\partial^2 E}{\partial \tau^a_{\kappa\alpha} \partial \tau^b_{\kappa'\beta}}. \quad (1)$$

Here, $\tau^a_{\kappa\alpha}$ is the displacement vector of the κth atom in the ath primitive unit cell (with translation vector $\mathbf{R}_a$) along the α axis. E is the Born-Oppenheimer (BO) total energy surface of the system (electrons plus clamped ions). The Fourier transform of the IFC's takes the following form:

$$\tilde{C}_{\kappa\alpha,\kappa'\beta}(\mathbf{q}) = \frac{1}{N}\sum_{a,b} C_{\kappa\alpha,\kappa'\beta}(a,b)\exp[-i\mathbf{q}\cdot(\mathbf{R}_a - \mathbf{R}_b)]$$
$$= \sum_b C_{\kappa\alpha,\kappa'\beta}(0,b)\exp(i\mathbf{q}\cdot\mathbf{R}_b). \quad (2)$$

The $\tilde{C}_{\kappa\alpha,\kappa'\beta}(\mathbf{q})$ include both ionic and electronic contributions. Each of these contributions is computed separately using DFPT.

The vibration frequencies ($\omega_{j,\mathbf{q}}$) and polarization vectors [$\mathbf{e}_\kappa(\mathbf{q}|j)$] of the phonon modes with wave vector $\mathbf{q}$ are determined by solving the eigenvalue matrix equation

$$\sum_{\kappa'\beta} \tilde{D}_{\kappa\alpha,\kappa'\beta}(\mathbf{q}) e_{\kappa'\beta}(\mathbf{q}|j) = \omega^2_{j,\mathbf{q}} e_{\kappa\alpha}(\mathbf{q}|j), \quad (3)$$

where $\tilde{D}_{\kappa\alpha,\kappa'\beta}(\mathbf{q})$ is the dynamical matrix, which is related to the Fourier transform of the IFC's according to the relation

$$\tilde{D}_{\kappa\alpha,\kappa'\beta}(\mathbf{q}) = \frac{1}{\sqrt{m_\kappa m_{\kappa'}}}\tilde{C}_{\kappa\alpha,\kappa'\beta}(\mathbf{q}). \quad (4)$$

Since ZnSe is a polar compound, the macroscopic electric field, caused by the long-range character of the Coulomb forces, contributes to the longitudinal optical phonons in the long-wavelength ($\mathbf{q}\to 0$) limit. This effect is included by calculating the nonanalytical part ($\tilde{C}^{na}$) of the force constants, given by[19]

$$\tilde{C}^{na}_{\kappa\alpha,\kappa'\beta} = \frac{4\pi e^2}{\Omega_0}\frac{\sum_{\beta'}(\mathbf{Z}^*_{\kappa,\beta'\alpha}q_{\beta'})\sum_{\alpha'}(\mathbf{Z}^*_{\kappa',\alpha'\beta}q_{\alpha'})}{\sum_{\alpha'\beta'} q_{\alpha'}\boldsymbol{\varepsilon}_{\infty_{\alpha'\beta'}}q_{\beta'}}. \quad (5)$$

Here, $\mathbf{Z}^*$ and $\boldsymbol{\varepsilon}_\infty$ are, respectively, the Born effective charges and the macroscopic high-frequency static dielectric tensors, which are also calculated self-consistently using DFPT.

B. Equation of state, thermal expansion, and heat capacity in the quasiharmonic approximation

The knowledge of the entire phonon spectrum of a given system enables the calculation of its thermodynamical properties and the relative stability of its different phases as functions of T. The thermodynamical properties are usually determined by the appropriate thermodynamical potential relevant to the given ensemble. In the ensemble where the sample volume (V) and T are independent variables, the relevant potential is the Helmholtz free energy (F). In the adiabatic BO approximation, F of a semiconductor can be written as

$$F = E + F_{\text{vib}} = E + E_{\text{vib}} - TS_{\text{vib}}, \quad (6)$$

where E_{vib} and S_{vib} is the contribution of the lattice vibration to the internal energy and entropy (S), respectively. The electronic entropy contribution to S, vanishes identically for insulators, and thus, it is not included in Eq. (7). Even for metals this contribution is usually neglected, although it is easy to calculate. Thus, the key quantity to calculate in order to have access to the thermal properties and to phase stability is F_{vib}.

The F_{vib} is usually calculated within quasiharmonic approximation (QHA).[20,24] This means calculating F_{vib} in the harmonic approximation, retaining only the implicit V dependence through the phonon frequencies, and it is given as[20]

$$F_{\text{vib}}(T,V) = k_B T\sum_{j,\mathbf{q}} \ln\{2\sinh[\hbar\omega_{j,\mathbf{q}}(V)/2k_B T]\}. \quad (7)$$

Here, $\omega_{j,\mathbf{q}}(V)$ is the phonon frequency of the jth phonon mode with wave vector $\mathbf{q}$ [inside the first Brillouin zone (BZ)] at fixed V, and k_B is the Boltzmann constant. The QHA accounts only partially for the effects of anharmonicity. However, QHA is found to be a very good approximation at temperatures not too close to the melting point.

For given T and V, the equilibrium state of a crystal is determined by minimizing F with respect of all possible degrees of freedom. The equation of state (P versus V) of the system is obtained by equating P to minus the derivative of F with respect to V at constant T, or

$$P = -\left(\frac{\partial F}{\partial V}\right)_T. \quad (8)$$

The thermal expansion is obtained directly from the equation of state, and the volume thermal expansion coefficient is defined as

$$\alpha_V = \frac{1}{V}\left(\frac{\partial V}{\partial T}\right)_P. \quad (9)$$

The linear thermal expansion coefficients for cubic crystals is given as

$$\alpha_a = \frac{1}{3}\alpha_V. \quad (10)$$

Due to anharmonicity effects, the heat capacity at constant P (C_P) is different from that at constant volume (C_V). The

former, which is what experiments determine directly, is proportional to T at high T, while the latter goes to a constant which is given by the classical equipartition law: $C_V=3Nk_B$ where N is the number of atoms in the system. The relation between C_P and C_V is[25]

$$C_P - C_V = \alpha_V^2(T)B_0VT, \tag{11}$$

where B_0 is the bulk modulus. Within QHA, C_V is given as[20]

$$C_V(T) = \sum_{\mathbf{q},j} c_{\mathbf{q},j}^V(T) = k_B \sum_{\mathbf{q},j} \left(\frac{\hbar\omega_{j,\mathbf{q}}(V)}{2k_BT}\right)^2 \frac{1}{\sinh^2[\hbar\omega_{j,\mathbf{q}}(V)/2k_BT]}, \tag{12}$$

where $c_{j,\mathbf{q}}^V(T)$ is the contribution to C_V of the $j,\mathbf{q}$ phonon mode at a certain T.

In practice, the summation over the phonon eigenstates, required to evaluate the above thermodynamic quantities, is transformed into integration over the phonon frequency.[24] This is because these thermodynamic quantities depend on $\mathbf{q}$ and j only through the frequency $\omega=\omega_{j,\mathbf{q}}$.

C. Computational details

Our calculations are performed employing the ABINIT package,[26,27] which is a self-consistent PPPW code.[28] For the exchange-correlation potential we have used the LDA data of Ceperly-Alder, as parametrized by Perdew and Zunger.[29] The wave functions are expanded in terms of plane wave (PW) basis sets with kinetic energy up to 65 and 35 Ryd for the 3d and NLCC calculations, respectively. Convergence tests have shown that increasing the cutoff energy of the 3d calculations to 75 Ryd, changes the phonon frequencies by less than 1 cm^{-1} and the equilibrium lattice parameter by less than 0.001 Å. The high cutoff used in the NLCC calculation is found necessary to get highly accurate phonon density of states $[g(\omega)]$ and, hence, accurate thermal properties. The integration over the BZ is done using a regular $4\times4\times4$ Monkhorst-Pack (MP)[30] mesh. Convergence tests have shown that this BZ sampling is sufficient to guarantee an excellent convergence (less than 1 cm^{-1}) of the calculated phonon frequencies.

The 3d calculations were performed by using a Se pseudopotential generated by employing Hamann's scheme,[31,32] and a Zn pseudopotential (with 3d electrons are included as valence states) constructed according to the Rappe *et al.*[33] optimization method. On the other hand, the NLCC calculations are performed by employing Zn and Se pseudopotentials generated following the Troullier-Martin scheme.[34] Ground state electronic configurations are used for both the Zn and Se atoms. The generated pseudopotentials are then transformed to the separable Kleinman-Bylander form.[35] All generated pseudopotentials are carefully tested and they are found to have excellent transferability are free from ghost states.[36]

The dynamical matrices were calculated, using DFPT, on a uniform grid in the first BZ. For a nonpolar material the dynamical matrix is analytic in reciprocal space and the IFC's are quite short ranged (i.e., negligible beyond a certain range $R_{\max}$). In this case, the IFC's can be obtained by Fourier transformation of the dynamical matrix computed on a discrete mesh in $\mathbf{q}$ space of spacing $\Delta q \leq 2\pi/R_{\max}$. The so-obtained IFC's can be used to compute the dynamical matrices at any arbitrary $\mathbf{q}$ point (i.e., a point not contained in the original grid). In case of a polar material, the dynamical matrix displays a nonanalytic behavior in the $\mathbf{q}\rightarrow0$ limit (see Sec. II). Therefore, the nonanalytic contribution [Eq. (5)] is subtracted from the dynamical matrix at each $\mathbf{q}$ point in the grid. Fourier transforming these modified dynamical matrices, gives the short-ranged IFC's. To compute the dynamical matrices at any $\mathbf{q}$ point, the above short-range IFC's are again Fourier transformed and added to the nonanalytic term. We found that a $4\times4\times4$ MP mesh (i.e., considering IFC's upto the ninth shell in real space) provides a very good convergence: Variations in the calculated phonon frequencies of less than 1 cm^{-1} are obtained by using a finer $8\times8\times8$ mesh (including IFC's up to the 25th nearest-neighbor shell). To compute the thermal properties one needs the phonon density of states, $g(\omega)$. The $g(\omega)$ calculations are carried out by employing the histogram method,[37] using 400 channels with a regular width of 5 cm^{-1}. In order to get a relative mean error smaller than 1% for all studied thermodynamical quantities, we found it is sufficient to sample the phonon wave vectors $\mathbf{q}$ by a $40\times40\times40$ MP mesh.

III. RESULTS AND DISCUSSION

A. Structural properties

We first determine the equilibrium volume of the ground state of the zinc-blende (ZB) phase of ZnSe by calculating the total energy per primitive unit cell as a function of V. The Murnaghan's equation of state[38] is then used to fit the calculated energy-volume data. The obtained structural parameters are compared in Table I with the available experimental data[4,39] and other theoretical results.[21,40–42] This table shows that our NLCC calculations underestimates the equilibrium lattice parameter (a_0) by 2.2% and overestimates the static bulk modulus (B_0) by 8.2% (with respect to experimental value of 64.7 GPa, see Table I). The relaxation of the semicore Zn 3d electrons improves significantly the calculated values of both a_0 and B_0: The relative error for a_0 and B_0 becomes 0.5 and 4.5 %, respectively. These errors are within the acceptable error bars due to the use of LDA,[21,22,40] which reflects the reliability of our self-consistent calculations, and the used pseudopotentials. It is worth noting that the NLCC results of Ref. 21 are in much better agreement with experiment than our NLCC results. This is because of the use of specially designed pseudopotentials, in Ref. 21, which take partially into account the relaxation of the semicore Zn 3d electrons: The considered Zn and Se pseudopotentials are *adjusted* linear combinations of several pseudopotentials generated using different ionic valence configurations. On the other hand, our NLCC calculations are standard ones (see Sec. II C).

Since we have access to the phonon frequencies, it is tempting to investigate the effects of zero-point motion on the structural properties of this system, although they are expected to be quite small. This gives us results for a_0 and B_0

TABLE I. Structural parameters of the ZB, SC16, and RS phases of ZnSe.

Phase	Method	a_0 (Å)	B_0 (GPa)	B_0'	u	v
ZB	Present work-3*d*	5.645	67.6	4.29		
	Present work-NLCC	5.543	70.0			
	PPPW-LDA-NLCC (Ref. 21)	5.662	65.0			
	PPPW-LDA (Ref. 40)	5.623	68.9	4.36		
	PPPW-LDA (Ref. 41)	5.606	70.5			
	LAPW-LDA (Ref. 42)	5.544	72.44	4.02		
	LAPW-LDA (Ref. 10)	5.568	71.4			
	LAPW-GGA (Ref. 10)	5.571	72.7			
	LMTO-LDA (Ref. 9)	5.633	81.1			
	SIESTA-LDA (Ref. 42)	5.666	62.45	4.05		
	Expt. (Ref. 39)	5.6676	64.7			
	Expt. (Ref. 4)	5.667	69.3			
SC16	Present work	6.905	73.74	4.45	0.1545	0.6425
	PPPW-LDA (Ref. 40)	6.881	63.9	5.5	0.1561	0.6421
RS	Present work	5.282	84.64	4.59		
	PPPW-LDA (Ref. 40)	5.268		4.28		
	LAPW-LDA (Ref. 42)	5.172	90.72	4.92		
	SIESTA-LDA (Ref. 42)	5.288	92.16	3.47		
	Expt. (Ref. 4)	5.299	104			

of 5.652 Å and 66.9 GPa, compared to those obtained without this correction of 5.645 Å and 67.6 GPa. This correction reduces the relative errors to 0.3 and 3.4 % for a_0 and B_0, respectively.

As a further check and in order to highlight the P range of interest, we have reinvestigated the structural phase transformation of ZnSe under high P. Our results for P_t of the ZB to RS (11.5 GPa) and ZB to SC16 (9.5 GPa) phase transitions are almost identical with those of Ref. 40. The SC16 phase has simple cubic unit cell with 16 atom basis. This shows that the first structural phase transformation (to SC16) is predicted to occur at 9.5 GPa. Experimentally, the observed first transition in ZnSe is to RS structure at about 13.5 GPa (see Ref. 4). Thus, the main P range considered in this work is between 0 and 9 GPa.

B. Elastic properties

The linear elastic constants are formally defined as $c_{\alpha\beta,\gamma\delta}=\partial\sigma_{\alpha\beta}/\partial\eta_{\gamma\delta}$, where $\boldsymbol{\sigma}$ and $\boldsymbol{\eta}$ denote the externally applied stress and the strain tensors, respectively. The fourth-rank tensor $\boldsymbol{c}$ has generally 21 independent components. However, this number is greatly reduced when taking into account the symmetry of the crystal. In the case of cubic crystals, there are only three independent elastic constants $c_{11}=c_{xx,xx}$, $c_{12}=c_{xx,yy}$, $c_{44}=c_{yz,yz}$. The c_{11}, c_{12} and unrelaxed (i.e., in absence of any internal displacement) c_{44} (c_{44}^0) elastic constants have been calculated by computing the second derivative of the BO energy surface with respect to the strain, namely, $c_{\alpha\beta,\gamma\delta}=\partial^2 E/\partial\eta_{\alpha\beta}\partial\eta_{\gamma\delta}$. This is performed at any V (or P) by employing the DFPT approach. The relaxed elastic constant c_{44} can be computed from the following relation:[43]

$$c_{44}=c_{44}^0-\frac{1}{4a_0}\mu\omega_{\mathrm{TO}}^2(\Gamma)\zeta^2, \tag{13}$$

where μ is the reduced atomic mass, $\omega_{\mathrm{TO}}(\Gamma)$ is the transverse-optical (TO) zone-center phonon frequency, and ζ is the internal-strain parameter that describes the relative sub-lattice displacement due to the macroscopic strain.[44] This quantity is also obtained using DFPT. As a check, the elastic constants are also calculated by the direct approach,[43] by imposing certain strain states and calculating the corresponding stress, and ζ is also directly determined—by force minimization. The results are shown in Table II. This table shows that direct and DFPT approaches give almost identical results, for both the elastic constants and ζ. Thus, in the following discussion only the DFPT results will be considered. For comparison, we give in Table II the available experimental data and other theoretical results.

The discrepancies between the present 3*d* value for ζ and the NLCC results are surprisingly quite large (of 13.6 and 22.5 % for the present and the Sörgel *et al.*[45] results, respectively). These discrepancies are, thus, mainly due to the relaxation of the Zn 3*d* electrons. On the other hand, our result with 3*d* electrons is in good agreement with the valence force model result.[46] The P variation of ζ (see Fig. 1) is appreciable and shows a sublinear behavior.

Table II shows that the 3*d* values for the elastic constants of ZnSe are in excellent agreement with the available experimental data.[47] The mean relative error at zero P is of 3, 7, and 8 % for c_{11}, c_{12}, and c_{44}, respectively. For c_{44}, it should be noted that a good agreement with experiment can be achieved after taking into account the effects of the internal-strain relaxation. Our calculated values including the semi-

TABLE II. Elastic constants (in GPa) and internal-strain parameter (ζ) of ZnSe. The superscript zero at c_{44} indicates the calculated values without taking into account the internal-strain relaxation. The experimental values of elastic constants are extrapolated to zero pressure (Ref. 45). VFM denotes the valence force field model.

	c_{11}	c_{12}	c_{44}	c_{44}^0	ζ
Present work-3d[a]	91.3	56.3	38.3	62.4	0.734
Present work-3d[b]	91.2	55.7	39.6	63.2	0.735
Present work-NLCC	96.2	59.9	52.7	70.6	0.634
PPPW-LDA-NLCC (Ref. 45)	97.8	52.5	47.0	63.1	0.569
LMTO-LDA (Ref. 9)	107.2	67.5	37.2		
VFM (Ref. 46)					0.723
ABCM (Ref. 8)	89.9	50.6	40.5		
Expt. (Ref. 58)	94.3	57.3	41.3		
Expt. (Ref. 47)	88.8	52.7	41.4		
Expt. (Ref. 59)	82.8	46.2	41.2		

[a]DFPT calculations.
[b]Direct calculations.

core states are in better agreement with experiment than those of previous NLCC,[45] our NLCC and LMTO[9] calculations. It is well known that the NLCC calculations overestimate the binding energy and highly underestimates a_0 (Ref. 48) and, hence, the overestimation of the elastic constants by this approach is understandable. The LMTO calculations[9] which are carried out by using the atomic sphere approximation (ASA) overestimate significantly the c_{11}, c_{12} elastic constants (and hence also the B_0, see Table I), while c_{44} is reasonably reproduced. It is well known[49] that ASA gives poor electric constants.

Figure 1 depicts the variation of the elastic constants of ZnSe with hydrostatic pressure, up to 9 GPa. It is evident that, within the P range of interest, c_{11} and c_{12} increase monotonically with P, whereas c_{44} shows a slight decrease. In the inset of Fig. 1, we compare the P variation of c_{11}, c_{12} and c_{44} in the 0–1 GPa pressure range, with available experimental data of Ref. 50. Our results for c_{44} and its P variation are in excellent agreement with experiment. For c_{11} and c_{12} the agreement with experiment is reasonable. However, their

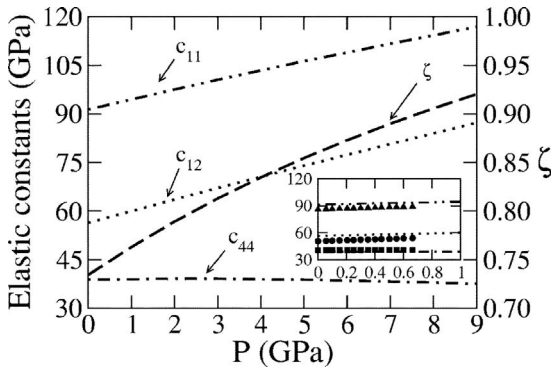

FIG. 1. Elastic constants and internal relaxation parameter (ζ) of ZnSe as functions of pressure. Triangles (c_{11}), circles (c_{12}), and squares (c_{44}) are the experimental values obtained at T=295 K, taken from Ref. 50.

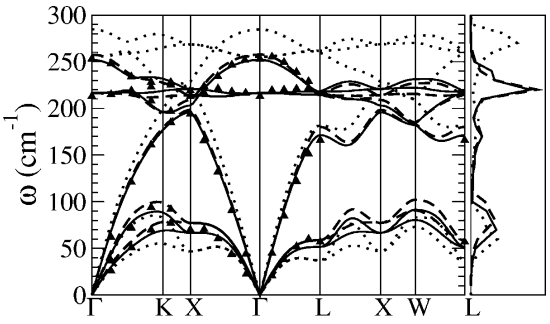

FIG. 2. Phonon spectra and density of states of ZnSe, at zero (solid lines) and 9 (dotted lines) GPa pressures. NLCC calculations at zero GPa are shown with dashed lines. The shown experimental data (triangles) obtained using INS at ambient pressure are taken from Ref. 2.

P variation shows a good agreement with experiments. The discrepancy in the case of c_{11} and c_{12} between our results and experiments is due to temperature effects. Indeed, the experimental data of Ref. 50 are obtained at 295 K. It is found theoretically, by *ab initio* calculations, that the elastic constants decrease upon temperature increase.[51] This is easy to understand from the fact that increasing T leads to an increase in the equilibrium volume, and, hence, to a decrease in the elastic constants. The better agreement we obtained for c_{44} is due to the weak P (and hence T) dependence of c_{44}, see Fig. 1. This behavior is consistent with that of MgO.[51]

C. Vibrational properties

The calculated phonon dispersion curves and density of states of ZnSe, at zero and 9 GPa pressures, are displayed in Fig. 2. There is no gap between the acoustical and optical phonon branches in $g(\omega)$, since there is a considerable overlap between the TO and longitudinal-acoustical (LA) phonon branches. This overlap is caused by the almost identical masses of Zn and Se atoms. One of the two TO phonon dispersion curves shows a considerable flatness along all high symmetry directions, which leads to a sharp peak in $g(\omega)$. From Fig. 2 it is evident that upon P increase the phonon spectra of the TA modes experience a downward shift while those of the other phonon modes are shifted upwards. This is consistent with the sign of their Grüneisen parameters, see below.

In Table III, we compare the phonon frequencies of some selected phonon modes with the available experimental data and other theoretical results. The features to note are as follows. (i) Our calculated phonon frequencies at zero P are in excellent agreement with the experimental data, obtained using INS.[2] The zone center TO phonon frequency ω_{TO}^{Γ} is slightly larger than the Raman spectroscopy data.[3] However, the zone center longitudinal-optical (LO) phonon frequency ω_{LO}^{Γ} is in excellent agreement with the Raman spectroscopy measurements.[3] (ii) The ω_{TO}^{Γ} calculated without including the Zn 3d electrons and without taking into account NLCC (Ref. 21) is much larger than the experimental value. (iii) Despite the differences between our NLCC calculations and those of Ref. 21 (see Sec. III A), they yield almost identical phonon

TABLE III. Dielectric constant, cation effective charge, and phonon frequencies (in cm^{-1}, at Γ, X, and L points) of ZnSe. BHS indicates calculation made with the pseudopotential of Ref. 32 (without NLCC).

	ε_∞	Z^*	ω_{TO}^{Γ}	ω_{LO}^{Γ}	ω_{TA}^{X}	ω_{LA}^{X}	ω_{TO}^{X}	ω_{LO}^{X}	ω_{TA}^{L}	ω_{LA}^{L}
Present work-3*d*	7.52	2.02	216	252	67	196	221	203	51	171
Present work-NLCC	6.59	2.00	217	258	74	198	214	209	59	180
DFPT-LDA-NLCC (Ref. 21)	6.3	2.01	219							
LAPW-LDA (Ref. 10)			198							
LAPW-GGA (Ref. 10)			206							
PPPW-LDA (Ref. 10)			203							
DFPT-LDA (Ref. 22)	6.66	2.057								
LMTO-LDA (Ref. 9)			224		79	173	203			
PPPW-BHS (Ref. 32)	5.9	1.78	238							
ABCM (Ref. 8)			219	253						
Expt.-INS (Ref. 2)			213	253	70	194	219	213	57	166
Expt.-Raman (Ref. 3)			204	252						
Expt. (Refs. 39 and 60)	6.3	2.03								

frequencies for the Γ_{TO} and Γ_{TO} modes which are, in turn, very close to the 3*d* results and experiment. (iv) Both the LDA and GGA results of the LAPW method[10] are in excellent agreement with Raman spectroscopy[3] for ω_{TO}^{Γ}, but shows a discrepancy with our value and with the INS data.

The P variation of some selected phonon frequencies of ZnSe is depicted in Fig. 3. The remarkable features to note from this figure are as follows (i) The TA modes at the X and L points, soften at a hydrostatic pressure of 16 GPa, well beyond the transition pressure (about 13.5 GPa). This shows that the observed ZB to RS structural phase transformation is due to thermodynamical instability rather than a dynamical one. This conclusion is consistent with RIM11 model calculations of Talwar *et al.*,[7] which do not show any softening of the ZnSe phonon modes up to 13.7 GPa. These results are in apparent contradiction with the conclusion of Karzel *et al.*,[4] obtained from the P dependence of the Lamb-Mössbauer factor, that soft phonon modes in ZnSe already appear at about 6 GPa. (ii) The LO-TO splitting at the Γ point decreases slightly with increasing P. (iii) By increasing P, the LA, LO, and TO show a monotonic increase in their phonon frequencies. However, the increasing rate is different for different $\mathbf{q}$ points in the BZ.

The P dependence of the phonon frequency is usually expressed in terms of the mode Grüneisen parameter

$$\gamma_{j,\mathbf{q}} = -(d \ln \omega_{j,\mathbf{q}}/d \ln V) = (B_0/\omega_{j,\mathbf{q}})(d\omega_{j,\mathbf{q}}/dp). \quad (14)$$

The $\gamma_{j,\mathbf{q}}$ parameters of ZnSe are shown in Fig. 4. In Table IV, we summarize our values for $\gamma_{j,\mathbf{q}}$ and $d\omega_{j,\mathbf{q}}/dP$ at some high symmetry points. We note that $\gamma_{j,\mathbf{q}}$ is strongly negative for almost the whole of the TA branches. This behavior is a common feature of the tetrahedral semiconductors.[20] Our calculated values for both $\gamma_{j,\mathbf{q}}$ and $d\omega_{j,\mathbf{q}}/dp$ are generally speaking in good agreement with experiment[3,52] and with other similar theoretical results.[22] A remarkable result of this study is the large downward shift of $\gamma_{j,\mathbf{q}}$ and $d\omega_{j,\mathbf{q}}/dp$ of the TA modes along the high symmetry lines, as shown in Fig. 4, arising from the relaxation of semicore Zn 3*d* electrons. Thus, these effects are expected to have important consequencies on the calculated thermal expansion (see Sec. III E 2). From Table IV, it is also clear that γ of the zone-center TO mode is larger than that of corresponding LO

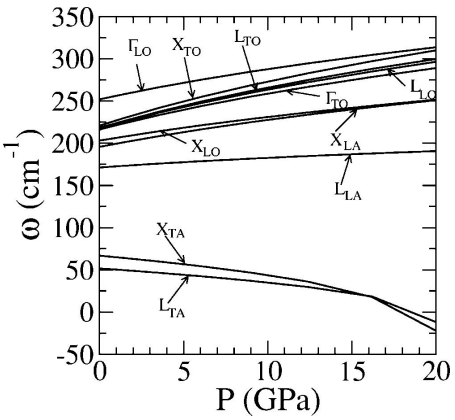

FIG. 3. Frequency of ZnSe phonon modes at some high symmetry points, as functions of pressure.

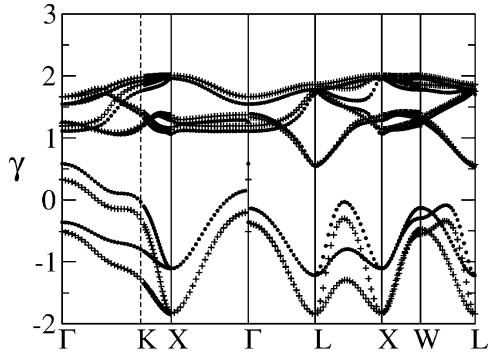

FIG. 4. Mode Grüneisen parameter of ZnSe, along several high symmetry directions of the fcc lattice. Circles: NLCC calculation. Crosses: 3*d* calculation.

TABLE IV. Grüneisen parameters γ_i and $d\omega_i/dp$ of ZnSe, at some high symmetry points.

	γ					$d\omega/dp$		
Mode	3*d*-Calc.[a]	NLCC-Calc.[a]	Calc.[b]	Expt.[c]	Expt.[d]	3*d*-Calc.[a]	NLCC-Calc.[a]	Expt.[d]
TO(Γ)	1.66	1.54	1.47	1.4	1.52	5.32	4.78	4.98
LO(Γ)	1.19	1.11	1.18	0.9	0.85	4.45	4.09	3.44
TO(*X*)	2.00	1.95	1.88	1.6		6.55	5.99	
LO(*X*)	1.14	1.06	1.04	0.9		3.42	3.17	
TO(*L*)	1.86	1.77	1.70	1.6		6.01	5.45	
LO(*L*)	1.75	1.70	1.63	0.9		5.64	5.17	
LA(*X*)	1.36	1.28	1.24	1.1		3.94	3.64	
TA(*X*)	−1.83	−1.11	−1.43	−1.3		−1.81	−1.22	
LA(*L*)	0.57	0.54	0.51	1.1		1.44	1.39	
TA(*L*)	−1.84	−1.21	−1.43	−1.5		−1.41	−1.02	

[a]Present work.
[b]LDA, DFPT calculation Ref. 22.
[c]Reference 52.
[d]Reference 3.

mode, which explains the decrease of the LO-TO modes splitting in ZnSe upon increasing P (see above).

D. Born effective charge and dielectric constant

In the ZB structure, the Born transverse effective charge tensor $\mathbf{Z}^*$ is isotropic. Because of the charge neutrality, the effective charge $Z^*=\frac{1}{3}\,\mathrm{Tr}\,\mathbf{Z}^*$ of the anions is minus that of the cations. The zero pressure value of Z^* of the cations is of 2.026 (2.00) for 3*d* (NLCC) calculation, which are in excellent agreement with the experimental value of 2.03 (see Table III). Although the calculated zero pressure value of $\varepsilon_\infty=\frac{1}{3}\,\mathrm{Tr}\,\boldsymbol{\varepsilon}_\infty$ with 3*d* electrons of ZnSe (7.53) is considerably higher that the experimental value (6.3), our NLCC value for ε (6.59) is in a good agreement with the experiment and other NLCC results,[21,22] see Table IV.

Figure 5 shows the calculated P dependence of Z^* and ε_∞. Both quantities show an appreciable decrease with increasing P, over the considered pressure range. The decrease in Z^* with increasing P is consistent with the decrease in the zone-center LO-TO splitting, see above, since they are directly related.[19] The Z^* variation is almost linear, while that of ε_∞ is relatively weaker and show a clear nonlinear behavior.

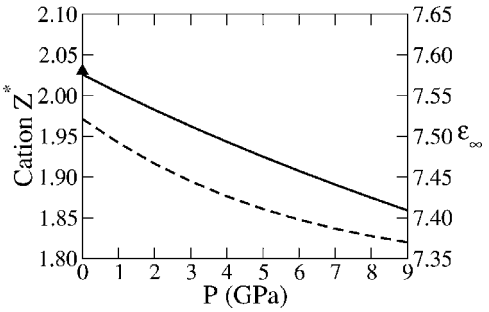

FIG. 5. Cation Z^* (solid line) and ε_∞ (dashed line) of ZnSe as functions of pressure.

E. Thermal properties

In the QHA, phonon frequencies depend on V, while intrinsic anharmonic effects arising from phonon-phonon interaction are neglected. These effects become more important at elevated T, and, hence, QHA becomes increasingly less adequate at high temperatures. However, anharmonic effects decrease with increasing pressure.[51] Indeed, the leading harmonic term in the expansion of the potential energy in terms of atomic displacement is expected to become increasingly predominant by decreasing V. Thus, the QHA generally works well over a wider temperature range at elevated pressures. In fact, for a stable crystal the QHA may be valid up to temperatures between the Debye (θ_D) and the melting (T_M) temperatures.[51,53] In some cases, especially in the presence of soft phonons, the QHA may fail even for temperatures below θ_D. For ZnSe, θ_D and T_M are, respectively, of 278 and 1800 K. Therefore, to avoid anharmonicity related effects, we consider in this work temperatures up to 400 K. As noted above, the considered pressure range is between 0 and 9 GPa.

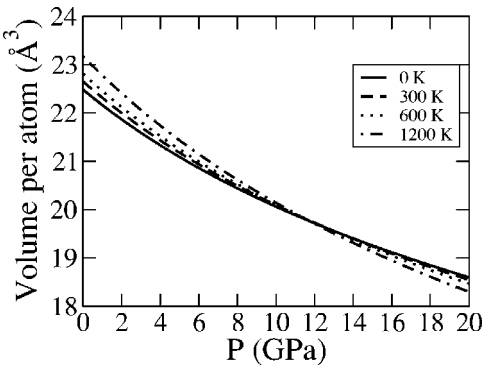

FIG. 6. Pressure-volume equation of state isotherms of ZnSe, at different temperatures.

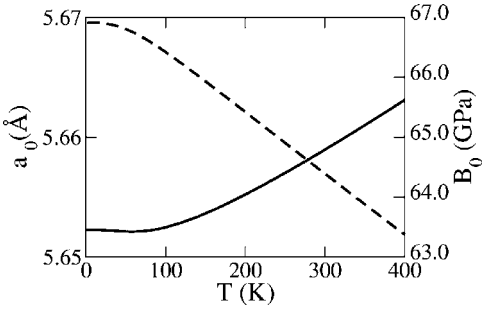

FIG. 7. Equilibrium lattice-parameter a_0 (solid line) and bulk modulus B_0 (dashed line) of ZnSe as functions of temperature.

1. Equation of state

The *P-V* equation of state (EOS) isotherms of ZnSe are depicted in Fig. 6. The shown EOS are determined by fitting the calculated Helmholtz free energy, at certain T, given by Eq. (9), to Murnaghan's EOS.[38] It can be seen that the volume of ZnSe decreases monotonically with P. At low P, higher temperature gives a larger $V(P)$ due to thermal expansion. By increasing P, the effects of the thermal expansion decrease, and beyond a critical value of P (about 12 GPa) $V(P)$ starts decreasing with increasing T. The a_0 and B_0 as functions of T (obtained from the fitting of F to Murnaghan's EOS) are shown in Fig. 7. We observe a slight decrease of a_0 in the T range of 0–60 K, indicating a negative thermal expansion, in agreement with experiment (see below). In this temperature range, B_0 experience a slight decrease. Above 60 K, a_0 (B_0) shows a monotonic increase (decrease) B_0 by increasing T. At room temperature, a_0 of the ZB phase of ZnSe increases by ~0.3% and B_0 decreases by ~4.7% with respect to the corresponding values obtained from static lattice calculations (Table I).

2. Thermal expansion

At zero P, the temperature variation of the linear thermal expansion coefficient, α_a, of ZnSe [determined using Eqs. (9) and (10)] is shown in Fig. 8. The available experimental results (at zero P) are also shown in the same figure. The most important features to note from this figure are as follows. (i) At low T, our results are in very good agreement with the experimental results of Smith *et al.*[6] The experimental results of Novikova[5] are significantly lower than our results and those of Smith *et al.*[6] To be more specific, we found that α_a is negative in the T range of 0–60 K, with a minimum value of -0.88×10^{-6} K^{-1} at 36 K. These results are in much better agreement with those of Ref. 6 (0–50 K, -0.68×10^{-6} K^{-1}, and 32 K, respectively) than those of Ref. 5 (0–60 K, $\sim-3\times10^{-6}$ K^{-1}, and 30 K). (ii) At higher temperatures (above 60 K), the experimental results agree with each other and with our 3*d* calculations. The so-obtained value of α_a at 283 K is 6.93×10^{-6} K^{-1}, which is in good agreement with the measured value of 6.84×10^{-6} K^{-1}.[6] (iii) Our NLCC results for α_a are in excellent agreement with experiment at low T. Above 50 K, these NLCC results are significantly smaller (6.44×10^{-6} K at 283 K) than experiment and our 3*d* calculations. The increase of α_a by relaxing the semicore electrons is quite unexpected, based on the downward shift of $\gamma_{j,\mathbf{q}}$ of the TA modes (see Sec. III C) and Eq. (15). However, one should note that $\gamma_{j,\mathbf{q}}$ is calculated for $\mathbf{q}$ points that lie along the high symmetry lines, while for calculating α_a an integration over the first BZ is required. (iv) Our NLCC results are in accord with the NLCC calculations of Ref. 22. It is worth noting again that our NLCC calculations are quite different from those of Ref. 22, which takes partially into account the relaxation of the semicore electrons (see Sec. III A). Thus, these results reflect the importance of the acutal relaxation of the semicore Zn 3*d* electrons for an accurate calculation of α_a.

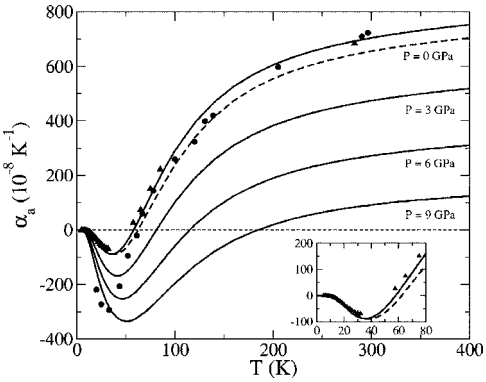

FIG. 8. Linear thermal expansion coefficient of ZnSe as a function of temperature, at different pressures. Triangles: experimental data of Ref. 6. Circles: experimental data of Ref. 5. Inset: data in the temperature range of 0–80 K, at zero P.

At high pressure, the α_a of ZnSe as a function of T is also shown in Fig. 8. Two important features can be noted from this figure: (i) α_a decreases notably by increasing P. At 300 K, for example, the value of α_a reduces from 7.04×10^{-6} K^{-1} to 0.92×10^{-6} K^{-1} by going from 0 to 9 GPa. (ii) The temperature range of negative α_a increases with P. At 9 GPa, α_a stays negative up to 180 K, compared to 60 K at zero P.The negative α_a at low T can be explained as follows. In the QHA, α_a can be written as[54]

$$\alpha_a(T) = \frac{1}{3B_0V}\sum_{j,\mathbf{q}} \gamma_{j,\mathbf{q}} c^V_{j,\mathbf{q}}(T). \tag{15}$$

At low T, the excited phonon modes are predominantly of TA type which have negative $\gamma_{j,\mathbf{q}}$ (see above), giving negative values of α_a. Moreover, as shown above, the hydrostatic pressure leads to a decrease in the frequency of the TA phonon modes and to an increase of that of the other modes. Thus, at high P and low T, the predominance of the TA phonon modes becomes increasingly more pronounced, leading to an increase in the range of T where α_a is negative and to a reduction in its calculated values. This behavior is similar to that obtained recently for ZnTe,[55] which indicates that this is a common feature for systems with negative α_a at low T.

3. Heat capacity

The calculated heat capacity at constant P, C_P, as a function of T is shown in Fig. 9, for different pressures. The available experimental results (at zero P) are also shown in

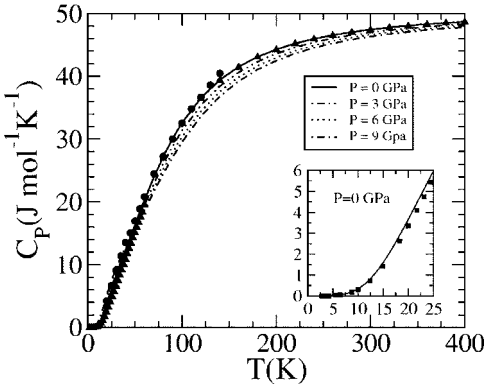

FIG. 9. As in Fig. 8, but for heat capacity at constant pressure. Triangles: NLCC calculations. Circles: experimental data of Ref. 57. Squares: experimental data of Ref. 56. Inset: data in the temperature range of 0–25 K, at zero P.

the same figure. It is evident that our results are in excellent agreement with the experimental data,[56,57] for the whole range of temperature considered experimentally. As for the P dependence of C_P, we note that at very low temperatures (below 50 K) C_P is almost insensitive to P, within the considered P range. Above this temperature, C_P is found to slightly decrease with increasing P. However at high temperatures, it becomes again insensitive to P. Finally, we note that the relaxation of the semicore Zn $3d$ electrons has negligible effects on $C_P(T)$, at zero pressure: our $3d$ and NLCC results are almost identical.

IV. CONCLUSIONS

We presented the results of a first-principles study of the pressure (P) dependence of the vibrational, thermal and elastic properties of ZnSe. Moreover, the P variation of the Born effective charge (Z^*) and high-frequency static dielectric constant (ε_∞) is investigated. The considered P and temperature (T) ranges are 0–9 GPa and 0–400 K, respectively. The calculations were performed employing a pseudopotential plane wave approach and the density functional perturbation theory, within the local-density approximation. In these calculations the semicore Zn $3d$ electrons are treated as valence states. Furthermore, some NLCC calculations have been performed for ZnSe, at zero pressure. Our calculated structural parameters, phonon spectra, elastic constants, Grüneisen parameter, linear thermal expansion coefficients α_a, and heat capacity at constant P, C_P, are generally speaking in very good agreement with the available experimental data and other similar theoretical calculations. The softening of the phonon modes is found to start at 16 GPa, above the transition pressure of the observed structural phase transformation to the rocksalt structure. This shows that such a transition is driven by a thermodynamical instability rather than a dynamical one. The temperature range of negative α_a is predicted to increase considerably with increasing P. Moreover, a strong decrease of α_a with P is predicted, for the whole temperature range considered. These results (for α_a) are consistent with what has been found for ZnTe, using model calculations, which suggests that these are common features for systems with negative α_a at low temperatures. The C_P is predicted to have a very weak P dependence, especially at very low and high temperatures. Appreciable P variation of both Z^* and $\boldsymbol{\varepsilon}_\infty$ is predicted. The importance of the relaxation of the semicore Zn $3d$ electrons is emphasized: it has considerable influence on the structural, elastic and thermal expansion properties — the phonon spectra and $C_P(T)$ are negligibly affected.

ACKNOWLEDGMENTS

Two of us (I.H and M.A) would like to thank the Center for Theoretical and Applied Physics, Yarmouk University, where part of this work was done, for financial support and kind hospitality.

[1] M. A. Haase, J. Qiu, J. M. DePuydt, and H. Cheng, Appl. Phys. Lett. **59**, 1272 (1991).
[2] H. Hennion, F. Moussa, G. Pepy, and K. Kunc, Phys. Lett. **35**A, 376 (1971).
[3] C.-M. Lin, D.-S. Chuu, T.-J. Yang, W.-C. Chou, J.-A. Xu, and E. Huang, Phys. Rev. B **55**, 13641 (1997).
[4] H. Karzel, W. Potzel, M. Köfferlein, W. Schiessl, M. Steiner, U. Hiller, G. M. Kalvius, D. W. Mitchell, T. P. Das, P. Blaha, K. Schwarz, and M. P. Pasternak, Phys. Rev. B **53**, 11 425 (1996).
[5] S. I. Novikova, Fiz. Tverd. Tela (Leningrad) **2**, 2341 (1960) [Sov. Phys. Solid State **2**, 2087 (1961)]; **3**, 178 (1961) [**3**, 129 (1961)]; **5**, 2138 (1963) [**5**, 1558 (1964)]; **1**, 1841 (1959) [**1**, 1687 (1960)].
[6] T. F. Smith and G. K. White, J. Phys. C **8**, 2031 (1975).
[7] D. N. Talwar, M. Vandevyver, K. Kunc, and M. Zigone, Phys. Rev. B **24**, 741 (1981).
[8] B. D. Rajput and D. A. Browne, Phys. Rev. B **53**, 9052 (1996).
[9] B. K. Agrawal, P. S. Yadav, and S. Agrawal, Phys. Rev. B **50**, 14881 (1994).
[10] A. V. Postnikov, O. Pagès, and J. Hugel, Phys. Rev. B **71**, 115206 (2005).
[11] S. Baroni, P. Giannozzi, and A. Testa, Phys. Rev. Lett. **78**, 1861 (1997).
[12] P. Giannozzi, S. de Gironcoli, P. Pavone, and S. Baroni, Phys. Rev. B **43**, 7231 (1991).
[13] N. E. Zein, Fiz. Tverd. Tela (Leningrad) (Leningrad) **26**, 3024 (1984) [Sov. Phys. Solid State **26**, 1825 (1984)].
[14] X. Gonze and J. P. Vigneron, Phys. Rev. B **39**, 13120 (1989).
[15] X. Gonze, D. C. Allan, and M. P. Teter, Phys. Rev. Lett. **68**, 3603 (1992).
[16] X. Gonze, Phys. Rev. A **52**, 1086 (1995).
[17] X. Gonze, Phys. Rev. A **52**, 1096 (1995).
[18] X. Gonze, Phys. Rev. B **55**, 10337 (1997).
[19] X. Gonze and C. Lee, Phys. Rev. B **55**, 10 355 (1997).

[20] S. Baroni, S. de Gioroncoli, and A. Dal Corso, Rev. Mod. Phys. **73**, 515 (2001).
[21] A. Dal Corso, S. Baroni, R. Resta, and S. de Gironcoli, Phys. Rev. B **47**, 3588 (1993).
[22] A. Debernardi and M. Cardona, Phys. Rev. B **54**, 11305 (1996).
[23] S. G. Louie, S. Froyen, and M. L. Cohen, Phys. Rev. B **26**, 1738 (1982).
[24] C. Lee and X. Gonze, Phys. Rev. B **51**, 8610 (1995).
[25] H. B. Callen, *Thermodynamics and an Introduction to Thermostatistics* (Wiley, New York, 1985).
[26] X. Gonze, J.-M. Beuken, R. Caracas, F. Detraux, M. Fuchs, G.-M. Rignanese, L. Sindic, M. Verstraete, G. Zerah, F. Jollet, M. Torrent, A. Roy, M. Mikami, Ph. Ghosez, J. Y. Raty, and D. C. Allan, Comput. Mater. Sci. **25**, 478 (2002).
[27] The ABINIT code is a common project of the Université Catholique de Louvin, Corning Incorporated, and other contributors, URL http://www.abinit.org
[28] W. E. Pickett, Comput. Phys. Rep. **9**, 115 (1989).
[29] J. P. Perdew and A. Zunger, Phys. Rev. B **23**, 5048 (1981).
[30] H. J. Monkhorst and J. D. Pack, Phys. Rev. B **13**, 5188 (1976).
[31] D. R. Hamann, Phys. Rev. B **40**, 2980 (1989).
[32] G. B. Bachelet, D. R. Hamann, and M. Schlüter, Phys. Rev. B **26**, 4199 (1982).
[33] A. M. Rappe, K. M. Rabe, E. Kaxiras, and J. D. Joannopoulos, Phys. Rev. B **41**, 1227 (1990).
[34] N. Troullier and J. L. Martins, Phys. Rev. B **43**, 1993 (1991).
[35] L. Kleinman and D. M. Bylander, Phys. Rev. Lett. **48**, 1425 (1982).
[36] X. Gonze, R. Stumpf, and M. Scheffler, Phys. Rev. B **44**, 8503 (1991).
[37] A. A. Maradudin, E. W. Montroll, C. H. Weiss, and I. P. Ipatova, *Theory of Lattice Dynamics in Harmonic Approximation*, 2nd ed. (Academic, New York, 1971), Chap. 4.
[38] F. D. Murnaghan, Proc. Natl. Acad. Sci. U.S.A. **30**, 244 (1944).
[39] *Semiconductors, Intrinsic Properties of Group IV Elements and III-V, II-VI, and I-VII Compounds*, edited by K. H. Hellwege and O. Madelung, Landolt-Börnstein, New Series, Group III, Vol. 22 Pt. a (Springer-Verlag, Berlin, 1982).
[40] A. Qteish and A. Muñoz, J. Phys.: Condens. Matter **12**, 1705 (2000).
[41] M. Coté, O. Zakharov, A. Rubio, and M. L. Cohen, Phys. Rev. B **55**, 13025 (1997).
[42] V. I. Smelyansky and J. S. Tse, Phys. Rev. B **52**, 4658 (1995).
[43] O. H. Nielsen and R. M. Martin, Phys. Rev. Lett. **50**, 697 (1983).
[44] L. Kleinman, Phys. Rev. **128**, 2614 (1962).
[45] J. Sörgel and U. Scherz, Eur. Phys. J. B **5**, 45 (1998).
[46] R. M. Martin, Phys. Rev. B **1**, 4005 (1970).
[47] B. H. Lee, J. Appl. Phys. **41**, 2984 (1970).
[48] G. E. Engel and R. J. Needs, Phys. Rev. B **41**, 7876 (1990).
[49] See, for example, X.-G. Zhang and D. M. C. Nicholson, Phys. Rev. B **60**, 4551 (1999).
[50] B. H. Lee, J. Appl. Phys. **41**, 2988 (1970).
[51] B. B. Karki, R. M. Wentzcovitch, S. de Gironcoli, and S. Baroni, Phys. Rev. B **61**, 8793 (2000).
[52] B. A. Weinstein, Solid State Commun. **24**, 595 (1977); *Proceedings of the Sixth High Pressure Science and Technology-AIRAPT Conference*, edited by K. D. Timmerhaus and M. S. Barker (Plenum, New York, 1979), Vol. I, p. 141.
[53] D. C. Wallace, *Thermodynamics of Crystals* (Wiley, New York, 1972).
[54] This equation is taken from K. Karch, P. Pavone, W. Windl, O. Schütt, and D. Strauch, Phys. Rev. B **50**, 17054 (1994). However, we found that the equation provided in this reference is incorrect: the division by V of the prefactor was missing.
[55] J. Camacho, I. Loa, A. Cantarero, and K. Syassen, J. Phys.: Condens. Matter **14**, 739 (2002).
[56] J. A. Birch, J. Phys. C **8**, 2043 (1975).
[57] J. C. Irwin and J. LaCombe, J. Appl. Phys. **45**, 567 (1974).
[58] V. I. Kuskov, A. P. Rusakov, and A. N. Menster, Sov. Phys. Solid State **14**, 1869 (1973).
[59] Y. A. Burenkov, A. A. Botaki, S. Y. Davydov, and S. P. Nikanorov, Sov. Phys. Solid State **19**, 1595 (1977).
[60] E. Burstein and G. Lucovsky, Int. J. Quantum Chem. **1**, 759 (1967).